Ultrasound monitoring of a deformable tongue-food gel system during uniaxial compression–an in vitro study

Rohit Srivastava, Mathieu Mantelet, Anne Saint-Eve, Jean-Luc Gennisson, Frederic Restagno, Isabelle Souchon, Vincent Mathieu

Ultrasound monitoring of a deformable tongue-food gel system during uniaxial compression–an *in vitro* study

Rohit SRIVASTAVA[a], Mathieu MANTELET[a], Anne SAINT-EVE[a], Jean-Luc GENNISSON[b], Frédéric RESTAGNO[c], Isabelle SOUCHON[d], Vincent MATHIEU[a]

[a]Université Paris-Saclay, INRAE, AgroParisTech, UMR SayFood,

F-78850, Thiverval-Grignon, France

[b]Université Paris-Saclay, CEA, CNRS, Inserm, BioMaps, Service Hospitalier Frédéric Joliot, 91401 Orsay, France

[c]Université Paris-Saclay, CNRS, Laboratoire de physique des solides, 91400 Orsay, France

[d]UMR 408 SQPOV, INRAE, Avignon Université, F-84000 Avignon, France

Submitted to: **Innovative Food Science and Emerging Technologies**

Declarations of interest: none

Corresponding author:

Vincent Mathieu

Paris-Saclay Food and Bio-product Engineering Laboratory (SayFood UMR 782)

Joint Research Unit INRAE AgroParisTech

Bâtiment CBAI

1, avenue Lucien Brétignières

78850 Thiverval-Grignon, France

Email: vincent.mathieu@inrae.fr

Phone: +33(0)1 30 81 68 13

Fax: +33(0)1 30 81 55 97

Abstract

This study presents a novel ultrasound method for exploring the mechanical deformability of artificial tongue models (ATMs) topped with agar and/or gelatin food gels during uniaxial compression. The ATMs were made from polyvinyl alcohol and displayed different levels of rigidity and surface roughness. We quantified deformation of the ATM-food system as it underwent compression induced by a texture analyzer. We collected real-time measurements via an ultrasound transducer (1 MHz) placed beneath the ATM, enabling to monitor non-invasively the ultrasound time of flight (ToF) and the apparent reflection coefficient (R*) of the ATM-food interface. The results on ToF reflected the tie between the level of force and ATM deformation; they were also precise enough to identify gel fracture. R* was a crucial parameter influenced by both ATM properties (rigidity, surface roughness) and food gel properties (syneresis, ability to mold to surface asperities).

Keywords

Food texture, Oral processing, Ultrasound, Artificial tongue models, Biomimetic set-up

1. Introduction

Food texture perception is the result of complex and dynamic phenomena, which occur simultaneously during food oral processing. Understanding the dynamics of texture perception is hence of paramount interest for food scientists who seek to understand and model consumers' sensorial experience of food (Renard, Van De Velde, & Visschers, 2006; Wilkinson, Dijksterhuis, & Minekus, 2000). As technological advances are made, new and more precise techniques for characterizing food properties (e.g., structure, rheology, and tribology) have been developed (Stokes, Boehm, & Baier, 2013). However, it remains difficult to precisely associate mechanical measurements with sensory attribute ratings and to follow texture dynamics during oral processing. The human oral cavity is very complex and equipped with different types of mechanoreceptors, which can detect both static and dynamic stimuli. The tongue is a crucial organ within the oral cavity: it moves food back and forth, facilitating proper mastication and the safe swallowing of boli. It also plays a very important role in texture perception, especially when food is compressed between the tongue and the palate (Ishihara et al., 2013; Kohyama, Ishihara, Nakauma, & Funami, 2021). During oral processing, the deformation of food over the tongue surface creates clusters of different stimuli, which are perceived by the mechanoreceptors and then sent to the brain for further processing, including texture determination. There is a growing body of literature that underscores how understanding the tongue's physiological properties can shed light on changes in food structure during oral processing and the resulting diversity of texture perceptions (Engelen & Van Der Bilt, 2008; Ketel, de Wijk, de Graaf, & Stieger, 2020; Van Vliet & Primo-Martín, 2011). Therefore, it is essential to further explore the dynamic interactions taking place between food and oral surfaces.

To effectively monitor such interactions, it is necessary to use a non-destructive technique that can be applied in real time. Ultrasound-based approaches have shown great promise and have been successfully employed to visualize tongue movement and bolus swallowing (Gao et al., 2013; Peng, Miethke, Pong, & Lin, 2007). Nevertheless, ultrasound images only provide qualitative information. Therefore, there has been a need to develop ultrasound-based methods with quantitative metrics

78 that can more precisely reveal the occurrence of events at the tongue-food interface. However,
79 quantifying the propagation of ultrasound waves in the human oral cavity can be quite difficult.
80 There is thus a need to develop an oral biomimetic set-up where the behavior of ultrasound waves
81 can be studied in a controlled manner. Mantelet, Restagno, Souchon, & Mathieu (2020) and
82 Mantelet, Srivastava, Restagno, Souchon, & Mathieu (2020) developed a novel ultrasound method
83 for analyzing the tongue-food interface *in vitro*; their research performed a detailed examination of
84 ultrasound reflectivity at the tongue-food interface, characterizing the effects of food properties,
85 lubrication, and tongue surface roughness. This proof-of-concept work utilized rough but non-
86 deformable tongue-mimicking surfaces made of polyvinyl chloride (PVC). It was found that the
87 reflectivity of ultrasound waves (as estimated via the apparent reflection coefficient, R*) at the
88 tongue mimic-food interface could be exploited to monitor changes in contact over time. This
89 research also clarified the influence of food properties and lubrication on R* and, thus, on interface
90 interactions.

91 However, the PVC tongue-mimicking surfaces did not very realistically recreate an actual human
92 tongue, and there was thus further room for improvement. Therefore, in this present article we have
93 introduced a novel artificial tongue-mimicking model (referred to as an ATM hereafter) made of
94 polyvinyl alcohol (PVA). In recent years, PVA has been used in biomedical engineering to model
95 arteries and oral mucosa (Chatelin et al., 2014; Fromageau et al., 2007; Gennisson et al., 2007; Jiang,
96 Liu, & Feng, 2011; Mamada, Fridrici, Kosukegawa, Kapsa, & Ohta, 2011). Tongue mimics made with
97 PVA were also used in our previous study dealing with oral tribology (Srivastava et al., 2021). PVA is a
98 water-soluble synthetic polymer and can be used to form hydrogels. The rigidity of PVA hydrogels
99 can be controlled by varying the number and kinetics of the freezing and thawing cycles (Fromageau
100 et al., 2007). This ability to control hydrogel rigidity made PVA a good fit for our study system.

101 The deformability of the PVA based ATM meant that it could be used in compression experiments in
102 which changes in tongue thickness over time were quantified using an ultrasound parameter called

time of flight (ToF). The data gathered helped reveal the relationships among tongue dynamics, food properties, and system deformation. Using the PVA based ATM, we also studied variability in R* in response to ATM properties (i.e., surface roughness, Young's modulus values, and water-release capacity) and food gel properties (i.e., Young's modulus values and water-release capacity), as such factors influence the tongue-food interface and, in turn, affect interactions between food and the tongue.

2. Materials and methods

2.1. Preparation and characterization of food gels

Preparation of the food gels

Eight different model gels (Table 1) made of agar and/or gelatin were prepared as described in Mantelet et al. (2020a and b). First, a sucrose solution (white sugar [Cristalco, Paris, France] dissolved in water) was prepared via stirring at 20 °C for 30 min. If needed, agar powder (HP700IFG, Kalys, Bernin, France) was incorporated, and the mixture was heated to 100 °C (until agar was completely dissolved) in a flask sealed with aluminum foil to limit any loss of water. After the agar powder was completely dissolved, the mixture was cooled to 60 °C. This temperature was maintained, and gelatin (Bloom 250 PS 8/3, Rousselot, Gent, Belgium) was added (if required); the mixture was continuously stirred for 20 min. Once the gelatin was completely dissolved, the solution was poured into cylindrical molds (30 mm in diameter, 10 mm in height) made of polyethylene and exposed to conditions promoting gelation (20 °C for 15–18 h). The gel was unmolded just before the experiment to prevent any loss of water or shape over time. Table 1 summarizes the mechanical properties of the gels, which were characterized during the aforementioned research.

Water-release capacity of the food gels

The water-release properties of these food gels were also quantified using a protocol adapted from Sala, Stieger, & van de Velde (2010). Three Whatman™ filter paper disks (110 mm diameter; GE

Healthcare Life Sciences, Chicago, USA) were placed on the base plate of a texture analyzer (TA.XT plus, Stable Micro Systems, Surrey, United Kingdom). A given gel was deposited on the disks and subjected to uniaxial compression (20% strain rate, 10 mm/s); there was a 5 s holding period. The maximum strain rate was chosen to avoid gel breakdown. The amount of water released was determined by comparing filter disk mass before and after the compression test. This methodology was somewhat modified in the case of the $Ag_{0.3}$ gel because the latter was very fragile and released water even without being compressed. Therefore, this gel was left on the filter disks for 5 sec and was then removed, without the application of any external stress. The paper was then weighed as in the case of the other gels. The results are presented in Table 1. However, in all future comparisons, we assumed that $Ag_{0.3}$ had highest water-release capacity.

2.2. Preparation and characterization of the artificial tongue models

Preparation of the artificial tongue models

First, PVA powder (Sigma Aldrich, Saint-Louis, USA) was dissolved in ultra-pure water (at 10% w/w) under stirring for 2 h at 80 °C. The solution was then cooled until it reached room temperature. The solution was subsequently poured into cylindrical molds (50 mm in diameter, 20 mm in height) that contained abrasive paper at the bottom. The choice of ATM thickness is based on values reported in literature which ranged from 10 mm to 40 mm (Nakamori et al., 2020; Beghini et al., 2017; Ishihara et al., 2013). To simulate two levels of surface roughness, two types of abrasive paper were used: (i) P80 sandpaper (grain size = 200 µm; Struers, Champigny-sur-Marne, France) and (ii) P40 sandpaper (grain size = 425 µm; Norton, Saint-Gobain, France). Hereafter, they are referred to as R_1 and R_2, respectively. The molds were sealed and frozen at -20 °C for 10 h. They were then thawed for 14 h at 20 °C. The freezing and thawing cycles were adjusted to attain the desired rigidity (Fromageau et al., 2007). Two types of ATMs were prepared: a soft ATM (C_2), which underwent two cycles, and a hard ATM (C_6), which underwent six cycles. After the completion of the requisite number of cycles, the

ATMs were unmolded and stored in reverse osmosis treated water at room temperature (20 °C) for several months.

Mechanical properties of the artificial tongue models

ATM rigidity was measured using uniaxial compression tests carried out with a texture analyzer (speed: 10 mm/s; strain rate: up to 20%; at least 3 replicates performed). This protocol was adapted from the work of Gao, Nakao, Ishihara, Funami, & Kohyama (2016). The resulting Young's modulus values are presented in Table 2.

Water-release capacity of the artificial tongue models

The ability of the ATMs to release water under mechanical compression was also quantified. For each ATM, any surface water was gently absorbed with Kimtech™ absorbent wipes (Kimberly-Clark, Irving, TX, USA) until the tissue came away dry. Subsequently, three layers of absorbing Whatman™ filter paper (110 mm diameter; GE Healthcare Life Sciences, Chicago, USA) were placed between the texture analyzer probe and the tongue's rough surface to fully collect the water released. We chose to use a strain rate of 5% and a holding time of 5 sec to avoid any damage to the tongue's surface from the aluminum probe. The difference in paper mass was then determined as previously described to estimate water-release capacity (Table 2).

Surface roughness profiles of the artificial tongue models

ATM surface roughness was analyzed via profilometry. Measurements were obtained using a contact profilometer (Dektak XT, Brucker, Billerica, MA, USA) with a 50-nm-radius stylus and 1 mg of applied force. For each ATM, three 30 mm surface scans were performed (one-dimensional, 45° of rotation between each scan). Vision 64 software (Bruker, Billerica, MA, USA) was used to control, analyze, and perform slope corrections before employing an algorithm in MATLAB (The MathWorks, Natick, Massachussetts, USA) to calculate roughness. Two parameters were chosen: the mean height of surface asperities (Ra) and correlation length, which is inversely related to asperity density (β).

175 Although only two types of sandpaper were used, the freezing and thawing cycles had an impact on
176 surface roughness as well. The values are presented in Table 2.

177 **2.3. Ultrasound measurements**

178 As in Mantelet et al. (2020a and b), the ultrasound set-up (Figure 1) comprised a texture analyzer, a
179 tongue-mimicking surface (a PVA based ATM in this study), and a mono-element piezoelectric
180 ultrasound transducer (central frequency of 1 MHz; V103RM, Olympus, Shinjuku, Tokyo, Japan); the
181 latter was placed beneath the ATM. Before starting each experimental test, the water on the surface
182 of the ATM was gently removed using absorbent wipes (Kimtech^{TM}, Kimberly-Clark, Irving, TX, USA)
183 until the tissue came away dry. The food gels were gently unmolded and placed on top of the ATM.
184 The texture analyzer was used to apply a controlled uniaxial deformation (of up to 8 mm at 10 mm/s)
185 to the ATM-food gel system using a circular aluminum probe (diameter: 40 mm). Ultrasound
186 measurements were made prior to the food being placed on the ATM (i.e., reference measurements)
187 and in real time during the compression period. To this end, the transducer, acting as both an emitter
188 and a receiver (pulse-echo mode), was used in tandem with a pulser-receiver (Sonatronic, Evry,
189 France). The pulser-receiver system was used to generate negative square wave pulses (width: 500
190 ns, amplitude: 80 V) and to digitize the radio frequency (*rf*) signals corresponding to the system's
191 pulse echo response (12-bit quantification, 100 MHz sampling rate, 38 dB gain). The frequency of
192 pulse recurrence was around 90 Hz. A LabVIEW (National Instrument, Austin, Texas, USA) interface
193 was used for real-time acquisition of the *rf* signals during the compression period.

194 **2.4. Signal processing**

195 Similarly to the work done in our previous research Mantelet et al. (2020a and b), the apparent
196 reflection coefficient of ATM-food interface (R*) was calculated on all the ultrasound signals of each
197 test. ATM deformability had an impact on both the amplitude and the time of occurrence of the
198 ultrasound waves reflecting off the ATM-food gel interface. The deformations induced during
199 compression shortened the path to be covered by the waves. As a consequence, the time needed for

200 the waves to travel between the emission source and back was shorter as well. Thus, in addition to
201 R*, here we have used another ultrasound parameter: time of flight (ToF).

202 Each experimental test is composed of a set of signals which have been analyzed using Matlab.
203 Figure 2a shows the typical shape of an *rf* signal, composed of two main echoes: E_0 for the tongue-
204 food interface, E_1 for the food-palate interface. Figure 2b shows the M-Mode representation of the
205 whole set of signals acquired during a test, where signal amplitude is coded in color and thus allows
206 to trace the evolution of the echoes identified in Figure 2a. For each signal, noise reduction was
207 implemented via a low-pass filter (cut-off frequency: 10 MHz). To precisely characterize ATM
208 deformation, it was crucial to accurately determine the ToF for the echo, E_0, associated with the
209 ATM-food gel interface over the entire course of a given test. E_1 echo was not processed for this
210 study. Using the reference signal, a time window was automatically defined; it had a width of 5 µs
211 and was centered with respect to the Hilbert-transformed peak amplitude of the signal. This window
212 of reference was then cross-correlated with all the *rf* signals acquired during a given test, allowing
213 the automatic detection of the ToF associated with E_0.

214 The ToF associated with the echo E_0 corresponds to the time required for the ultrasonic wave to
215 return to the sensor after being reflected at the interface between the ATM and the food. The
216 thickness (e) of the ATM is proportional to this time of flight ToF:

217 $$e = \frac{1}{2}.ToF.c$$

218 Where c is the propagation speed of ultrasound waves in the 10% PVA hydrogels (1540 m/s at 20 °C;
219 Gennisson et al., 2007). Finally, the deformation of the ATM (Δe) was deduced by subtracting the real
220 time thickness (e) of the ATM from its initial value e_0. As an example for validation of the accuracy of
221 the method, we compared it with deformation measurements assessed with the texture analyzer. To
222 do so, we considered the compression of an ATM without any food. The deformation applied was
223 20%, with a velocity equal to 10 mm/s (similarly to as done for the tests in presence of food). Three

repetitions were performed. The obtained average curves with standard deviation envelopes can be compared in Figure 3. The obtained graphs hence show that the deformation measurements by both ultrasound and texture analyzer are in agreement, confirming the relevance of the ultrasound velocity value (1540 m/s) used for the calculation, and validating the method for tongue deformation assessment.

To reliably calculate R* at the ATM-food gel interface, it was necessary to accurately estimate the amplitude of E_0. For all the *rf* signals, time windows encompassing E_0 had a width of 5 µs and were defined so as to be centered around the ToF for E_0. A Hanning window was applied, and the amplitude of E_0 was defined as the maximum amplitude of the power spectrum (the Fourier transform of the autocorrelation function) for the window obtained. R* was defined as E_0's amplitude during a given test, expressed as a percentage of E_0's amplitude during the reference measurements (i.e., when there was no food gel on the ATM). Consequently, the evolution of ToF and R* were computed for the entire duration of an experimental test, as illustrated in Figure 2c which focuses on the compression step.

3. Results and discussion

To begin with, the biomimetic set-up with different ATMs was developed. The roughness and rigidity values (Table 2) of the ATMs fabricated for this study were found to be in accordance with the values reported for real human tongues. Ishihara et al., (2013) has reported the rigidity of the human tongue at rest as 12.2 ± 4.2 kPa and at contracted state as 122.5 ± 58.5 kPa. Moreover, the surface asperities height (filiform papillae) of human tongue was reported between 50 - 150 µm (Andablo-Reyes et al., 2020; Wang, Wang, Upadhyay, & Chen, 2019). Also, Andablo-Reyes et al. (2020) reported average diameter of filiform papillae around 350 µm. Hence the characteristics of the developed ATMs were in good accordance with the values published in literature on human tongues.

The results and discussion on these ATMs are discussed below and have been structured into two main parts that each focus on one of ultrasound parameters: (i) ToF and (ii) R*.

3.1. Characterizing the deformation of the artificial tongue models—ToF

It is important to investigate the deformation of the tongue during oral processing because this phenomenon can directly change food bolus characteristics and stimulate the mechanoreceptors responsible for texture perception. In this study, our *in vitro* approach allowed us to measure the ToF of the ultrasound waves reflected off of the ATM-food gel interface, providing an accurate estimate of ATM deformation during the uniaxial compression of the system. The maximum possible degree of ATM deformation (in the absence of food) was 40% because initial ATM thickness was 20 mm, and the level of deformation applied to the system was fixed at 8 mm. It is also important to have in mind that the diameter of the ultrasound beam (less than 10 mm) is lower than the diameter of the gels. Thus, the deformations measured by ultrasound only reflect what is happening in the central part of the ATM, which can be assumed as planar.

Effect of food properties

When the soft (C_2R_2) ATM was used, varied profiles of force (as measured by the texture analyzer) were observed over the range of food gels (plate displacement: 8 mm at 10 mm/s; Figure 4a). The ToF values obtained during these experimental tests showed that ATM deformation changed over time (Figure 4b). Force and ATM deformation showed similar trends. When tests were performed using the hard (C_6R_2) ATM, we saw the same patterns and similarity in metric values (Figures 4c and 4d). These results are encouraging because they underscore the relationship between ATM deformation and the force applied to the system during compression. The *in situ* and non-invasive characterization made possible here with ultrasound gives promising long term *in vivo* perspectives. Forces and deformations indeed constitute very relevant information to monitor during oral processing, but they remain impossible to characterize so far. The ToF values also showed that it was possible to identify the fracture point of food gels during compression. Like the level of force, tongue deformation was found to be sensitive to the sudden breakage of food gels. Out of the eight food

gels, $Ag_{0.3}$ was the only one that fractured during compression, and this event was easily observed in both the ATM deformation results and the force results.

It is also clear from the results that ATM deformation was affected by the mechanical properties of the food gels. For example, because $Ag_{0.3}$ and $Ge_{3.5}$ were softer, they did not cause as much ATM deformation as did the more rigid food gels like $Ag_{1.8}$. To understand this phenomenon, it is useful to make the comparison with the situation of two springs connected in series. Total deformation is the sum of the strains experienced by the individual springs. Hence, the softer gels more equally shared the deformation resulting from system compression, whereas the more rigid gels did not, leading the ATM to deform more in compensation.

Effect of artificial tongue model properties

The human tongue is a complex muscular organ that is also a hydrostat. In other words, its volume remains constant when its rigidity is modulated or when it is in motion (Napadow, Chen, Wedeen, & Gilbert, 1999). Tongue rigidity changes considerably over the course of oral processing to better manage the bolus and texture perception. We used the PVA based ATM to investigate the role of rigidity in food deformation. We measured force and ATM deformation during experimental tests in which the different food gels were placed on the soft and hard ATMs (C_2R_2 and C_6R_2, respectively; values following compression: Figure 5). ATM rigidity affected the relationship between the level of force and ATM deformation. For both ATM types, the different food gels formed clusters that were based on the gels' mechanical properties). It represents that the diversity in mechanical property of gels were suitable for this study. Some food gels, like $Ag_{0.3}$, resulted in little tongue deformation, while others, like $Ag_{1.8}$, led to nearly 8 mm in deformation in the soft ATM, suggesting that the food gels themselves were not deformed at all. Taken together, the clusters of points for each ATM type followed a specific pattern, which was comparable to the curves obtained for the Young's modulus values during ATM compression. It is thus evident that the hard ATM led to greater force than did the soft ATM. Moreover, ATM rigidity also influenced food deformation kinetics. Using $Ag_{0.3}$ as an

example, both the force and ATM deformation results show that gel fracture occurred earlier on the hard ATM than on the soft ATM (Figure 4). These results highlight that ATM rigidity plays an important part in shaping the extent and kinetics of food deformation.

The human tongue has a particular surface topology due to the presence of different papillae. However, the latter's role in the bulk deformation of food has yet to be thoroughly explored. In this study, force and ATM deformation displayed different patterns over time when certain food gels (notably gelatin-dominant gels) were placed on ATMs with the same rigidity but different surface roughness. For example, in case of the gelatin-dominant gels $Ge_{3.5}$ and Ge_{7}, the effect of surface roughness on tongue deformation was much more pronounced for the hard ATM (Figures 6a, b), since the deformation curve for C_6R_1 was more distant from C_6R_2 when comparing C_2R_1 with C_2R_2. The explanation could be that, when the cylindrical gels were compressed on top of the ATM, a barreling effect arose from friction and adhesion coming into play (Brennan & Bourne, 1994; Pons & Fiszman, 1996). Barreling effects occur when there is friction between a plate and a specimen, which results in a state of triaxial stress instead of the ideal state of uniaxial stress. Since gelatin polymers have adhesive properties and release less water, the degree of friction might have been greater. The agar-dominant gels did not display such a pattern, perhaps because of their higher degree of water release.

This explanation could also apply to the results for the hard ATM, which released less water during compression. Furthermore, the number of freezing and thawing cycles positively affected mean peak asperity height (Table 2). The presence of taller asperities with negligible water in the interphase region should have enhanced adhesion between the food gels and the ATM. Greater adhesion can enhance barreling effects, lowering the uniaxial force exerted on the system.

3.2. Analysis of the tongue model-food gel interface—R*

R* is the parameter used to quantify the apparent reflection of ultrasound waves at the interface between the ATM and the food gels, and its value is greatly dependent on the media's difference in

acoustic impedance (Mantelet et al., 2019). R* has been shown to be a key parameter for understanding the characteristics of the tongue-food interface (Mantelet et al., 2020a and b). More specifically, it was found that there was a pronounced difference in acoustic impedance between a PVC tongue-mimicking surface and various food gels, resulting in the strong reflection of ultrasound waves at the interface. Here, in contrast, the PVA based ATM and the food gels appeared to have similar acoustical impedance, PVA being thus more representative of the acoustic properties of human soft tissue. However, it may also mean that the quantity of acoustic energy reflected by the ATM-food gel interface was limited. That said, there were clear differences in R* among food gels (Figure 7a). Results for the C_2R_2 ATM underscore the sensitivity of our ultrasound method when it comes to analyzing the interface between the PVA ATM (with its more biologically realistic properties) and the food gels. Previous research has examined variation in R* for a PVC tongue-mimicking surface (Mantelet et al., 2020a and b). The presence of trapped air at the interface was found to be a key factor affecting R* variations. The value of this parameter was at a minimum when no air was present, representing a state of perfect coupling between the ATM and food gel; in contrast, when R* was maximum, coupling was imperfect due to significant amounts of trapped air. Factors that can alter air presence are water release or mechanical deformation. The results obtained here were similar to those seen in the previous study. R* values varied depending on food gel type and the amount of water present at the interface.

Effect of food gel properties

Polymers like agar or gelatin form very different structures upon gelation, resulting in products that differ in rigidity and water-release capacity (Santagiuliana, Piqueras-Fiszman, van der Linden, Stieger, & Scholten, 2018). Consequently, we observed a variety of changes in R* over time: it decreased, plateaued, or increased over the course of compression, indicating the presence of a nonlinear response. It was therefore necessary to study the data quantitatively. When the values of R* were examined and compared for two time points (Figure 7b), t_0 (test begins—food gel is deposited on the

ATM) and t_1 (test ends following the compression period), it was evident that two main factors were at play. Syneresis and the gel's ability to mold itself to ATM surface asperities appeared to govern changes in R* over time.

At t_0 (Figure 7b), the R* value for $Ag_{0.3}$ was quite low since the latter was an extremely soft food gel that released a large amount of water, improving contact with the ATM's surface. $Ge_{3.5}$ had a comparatively higher R* value despite its nearly equivalent Young's modulus value because it released less water. The values at t_0 can shed some light on why some food gels might be perceived as dry or wet when deposited on the tongue.

When the food gels were compressed on the ATM, the main trend observed was a decrease of R* since the application of stress tended to improve contact at the interface. The R* values following compression (t_1) provided much needed insight into the role of food gel and ATM properties in predicting the degree of improvement in contact. The higher the gel's gelatin concentration, the higher the initial R* value, suggesting poorer levels of contact. There was thus greater room for improvement when the uniaxial stress was applied. This difference was starker for the more rigid gelatin-dominant gels since the force exerted to achieve 8 mm in deformation was much higher, resulting in better contact between the food gel and the ATM.

Effect of artificial tongue model properties

ATM properties also influenced the R* values. When examining how ATM rigidity type (C_2R_2 = soft and C_6R_2 = hard) affected the results obtained with the food gels $Ag_{0.3}$, $Ge_{3.5}$, Ge_7, and Ge_{7T}, it was found that R* was higher at the start of the tests (t_0) for C_6R_2 compared to C_2R_2 (Figures 8a and 8b). The greater the number of freezing-thawing cycles, the denser and more rigid the PVA becomes, affecting the polymer's ability to release water. The resulting absence of water at the interface could explain why R* was higher for the C_6R_2 ATM. As discussed previously, low levels of lubrication at the interface can augment adhesion, resulting in a barreling effect and an uneven decline in compression force. This barreling effect might lead to uneven surface deformation as well as air pockets, thus

increasing R*. Another explanation could be that the hard ATM underwent six cycles of freezing and thawing, more greatly affecting its surface roughness (peak height) even though sandpaper grain size was the same. Increased asperity height could have led to more air being trapped at the interface, boosting R* values.

When rigidity was controlled, ATM surface roughness (C_2R_1 vs. C_2R_2) was found to affect R* values (Figures 9a and 9b): it resulted in different temporal patterns in R* for the three gelatin-dominant gels ($Ge_{3.5}$, Ge_7, Ge_{7T}). R* values were higher for C_2R_1 than for C_2R_2, which was an unexpected result because one would assume that higher asperities would lead to more trapped air, enhancing wave reflection. However, it should also be noted that, compared to C_2R_1, C_2R_2 had a larger peak correlation length (β) (i.e., wider peaks) and hence a lower peak density. Peak density could affect surface topography overall, potentially explaining this unexpected observation.

The comparison of the R* values for Ge_7 versus Ge_{7T} sheds light on the ability of TWEEN to modify interface characteristics (Figure 9c). As a surfactant, TWEEN lowers the surface tension of water, promoting its spread under conditions of compression and expelling the air trapped among asperities. It seems likely that the properties of the surfactant in Ge_{7T} reduced the difference in the R* values when this food gel was used on ATMs of different surface roughness.

4. Conclusions

In this study, we used PVA based ATMs with different bulk rigidities and surface roughness profiles to investigate the role of tongue deformability in the mechanical compression of food gels by a hard palate. The ToF of the ultrasound wave traveling to and from the ATM-food gel interface was used as a key metric for characterizing the overall deformation of the system. The ToF values helped estimate ATM deformation during the uniaxial compression of the food gels and were found to fit with the force exerted on the system. R*, or the apparent reflection coefficient, has been employed in previous studies to analyze tongue-food dynamics. It was found to be effective here as well for

characterizing real-time changes at the ATM-food gel interface over the course of compression, including changes in the relationship between contact dynamics and both gel properties (i.e., Young's modulus values, water-release capacity) and ATM properties (i.e., deformability and surface roughness). More importantly, this study demonstrated that, despite the similarities in the acoustical impedance of the ATMs and the food gels, it was possible to accurately quantify reflection at a rather small scale. Consequently, this approach may hold promise for *in vivo* applications involving biological tissues and food, which have similar acoustical properties.

The study also underscored the utility of PVA in ATM design, given that it is a material that can better replicate tongue rigidity and roughness, a need that still exists in food oral processing research. Additionally, our findings showed that ultrasound techniques could be useful for tracking quantitative information related to mechanical interactions between the tongue and the palate.

Future work using this set-up will focus on investigating how ultrasound indicators respond when investigating systems with more complex, heterogeneous model foods. The broader goal is to progressively bridge the gap between model food and real food. Future research will also better account for the complexity of food oral processing, a greater diversity of motion (mixing shearing and compression) will be simulated and tongue shape, oral cavity anatomy and oral temperature will be more realistically recreated to further put ultrasound techniques to the test, prior to their more widespread use *in vivo*.

Acknowledgments

We wish to acknowledge the crucial technical support provided by David Forest and Mary Ugwonali. We are grateful to Sandrine Mariot for her help with the profilometry measurements. We also thank Jessica Pearce-Duvet for proofreading this manuscript.

Funding

This work was financially supported by the QUSToFood project funded by the French National Research Agency (ANR-17-CE21-004).

References

Beghini, M., Pereira, T. L., Montes, J. M. C., De Moura, D. V., Dezem, T. U., …. De Lima Pereira, S. V. (2017). Morphometric Analysis of Tongue in Individuals of European and African Ancestry. *Journal of Forensic Investigation*, *5*(1). https://doi.org/10.13188/2330-0396.1000038

Andablo-Reyes, E., Bryant, M., Neville, A., Hyde, P., Sarkar, R., Francis, M., & Sarkar, A. (2020). 3D Biomimetic Tongue-Emulating Surfaces for Tribological Applications. *ACS Applied Materials and Interfaces*, *12*(44), 49371–49385. https://doi.org/10.1021/acsami.0c12925

BRENNAN, J. G., & BOURNE, M. C. (1994). Effect of Lubrication on the Compression Behaviour of Cheese and Frankfurters. *Journal of Texture Studies*, *25*(2), 139–150. https://doi.org/10.1111/j.1745-4603.1994.tb01322.x

Chatelin, S., Bernal, M., Deffieux, T., Papadacci, C., Flaud, P., Nahas, A., … Pernot, M. (2014). Anisotropic polyvinyl alcohol hydrogel phantom for shear wave elastography in fibrous biological soft tissue: A multimodality characterization. *Physics in Medicine and Biology*, *59*(22), 6923–6940. https://doi.org/10.1088/0031-9155/59/22/6923

Engelen, L., & Van Der Bilt, A. (2008). Oral physiology and texture perception of semisolids. *Journal of Texture Studies*, *39*(1), 83–113. https://doi.org/10.1111/j.1745-4603.2007.00132.x

Fromageau, J., Gennisson, J. L., Schmitt, C., Maurice, R. L., Mongrain, R., & Cloutier, G. (2007). Estimation of polyvinyl alcohol cryogel mechanical properties with four ultrasound elastography

methods and comparison with gold standard testings. *IEEE Transactions on Ultrasonics, Ferroelectrics, and Frequency Control*, *54*(3), 498–508. https://doi.org/10.1109/TUFFC.2007.273

Gao, Z., Nakao, S., Ishihara, S., Funami, T., & Kohyama, K. (2016). A Pilot Study on Ultrasound Elastography for Evaluation of Mechanical Characteristics and Oral Strategy of Gels. *Journal of Texture Studies*, *47*(2), 152–160. https://doi.org/10.1111/jtxs.12170

Gennisson, J.-L., Rénier, M., Catheline, S., Barrière, C., Bercoff, J., Tanter, M., & Fink, M. (2007). Acoustoelasticity in soft solids: Assessment of the nonlinear shear modulus with the acoustic radiation force. *The Journal of the Acoustical Society of America*, *122*(6), 3211–3219. https://doi.org/10.1121/1.2793605

Ishihara, S., Nakao, S., Nakauma, M., Funami, T., Hori, K., Ono, T., … Nishinari, K. (2013). Compression Test of Food Gels on Artificial Tongue and Its Comparison with Human Test. *Journal of Texture Studies*, *44*(2), 104–114. https://doi.org/10.1111/jtxs.12002

Jiang, S., Liu, S., & Feng, W. (2011). PVA hydrogel properties for biomedical application. *Journal of the Mechanical Behavior of Biomedical Materials*, *4*(7), 1228–1233. https://doi.org/10.1016/j.jmbbm.2011.04.005

Ketel, E. C., de Wijk, R. A., de Graaf, C., & Stieger, M. (2020). Relating oral physiology and anatomy of consumers varying in age, gender and ethnicity to food oral processing behavior. *Physiology and Behavior*, *215*(August 2019), 112766. https://doi.org/10.1016/j.physbeh.2019.112766

Kohyama, K., Ishihara, S., Nakauma, M., & Funami, T. (2021). Fracture phenomena of soft gellan gum gels during compression with artificial tongues. *Food Hydrocolloids*, *112*(August 2020), 106283. https://doi.org/10.1016/j.foodhyd.2020.106283

Mamada, K., Fridrici, V., Kosukegawa, H., Kapsa, P., & Ohta, M. (2011). Friction properties of poly(vinyl alcohol) hydrogel: Effects of degree of polymerization and saponification value. *Tribology Letters*, *42*(2), 241–251. https://doi.org/10.1007/s11249-011-9768-8

Mantelet, M., Panouillé, M., Boué, F., Bosc, V., Restagno, F., Souchon, I., & Mathieu, V. (2019). Impact of sol-gel transition on the ultrasonic properties of complex model foods: Application to agar/gelatin gels and emulsion filled gels. *Food Hydrocolloids*, *87*(May 2018), 506–518. https://doi.org/10.1016/j.foodhyd.2018.08.021

Mantelet, M., Restagno, F., Souchon, I., & Mathieu, V. (2020). Using ultrasound to characterize the tongue-food interface: An in vitro study examining the impact of surface roughness and lubrication. *Ultrasonics*, *103*(April 2019), 106095. https://doi.org/10.1016/j.ultras.2020.106095

Mantelet, M., Srivastava, R., Restagno, F., Souchon, I., & Mathieu, V. (2020). Real time ultrasound assessment of contact progress between food gels and tongue mimicking surfaces during a compression. *Food Hydrocolloids*, 106099. https://doi.org/10.1016/j.foodhyd.2020.106099

Nakamori, M., Imamura, E., Fukuta, M., Tachiyama, K., Kamimura, T., Hayashi, Y., … Wakabayashi, S. (2020). Tongue thickness measured by ultrasonography is associated with tongue pressure in the Japanese elderly. *PLoS ONE*, *15*(8 July), 1–12. https://doi.org/10.1371/journal.pone.0230224

Napadow, V. J., Chen, Q., Wedeen, V. J., & Gilbert, R. J. (1999). Intramural mechanics of the human tongue in association with physiological deformations. *Journal of Biomechanics*, *32*(1), 1–12. https://doi.org/10.1016/S0021-9290(98)00109-2

Pons, M., & Fiszman, S. M. (1996). Instrumental texture profile analysis with particular reference to gelled systems. *Journal of Texture Studies*, *27*(6), 597–624. https://doi.org/10.1111/j.1745-4603.1996.tb00996.x

Renard, D., Van De Velde, F., & Visschers, R. W. (2006). The gap between food gel structure, texture and perception. *Food Hydrocolloids*, *20*(4), 423–431. https://doi.org/10.1016/j.foodhyd.2005.10.014

Sala, G., Stieger, M., & van de Velde, F. (2010). Serum release boosts sweetness intensity in gels.

Food Hydrocolloids, *24*(5), 494–501. https://doi.org/10.1016/j.foodhyd.2009.12.001

Santagiuliana, M., Piqueras-Fiszman, B., van der Linden, E., Stieger, M., & Scholten, E. (2018). Mechanical properties affect detectability of perceived texture contrast in heterogeneous food gels. *Food Hydrocolloids*, *80*, 254–263. https://doi.org/10.1016/j.foodhyd.2018.02.022

Srivastava, R., Bosc, V., Restagno, F., Tournier, C., Menut, P., Souchon, I., & Mathieu, V. (2021). A new biomimetic set-up to understand the role of the kinematic, mechanical, and surface characteristics of the tongue in food oral tribological studies. *Food Hydrocolloids*, *115*(July 2020). https://doi.org/10.1016/j.foodhyd.2021.106602

Stokes, J. R., Boehm, M. W., & Baier, S. K. (2013). Oral processing, texture and mouthfeel: From rheology to tribology and beyond. *Current Opinion in Colloid and Interface Science*, *18*(4), 349–359. https://doi.org/10.1016/j.cocis.2013.04.010

Van Vliet, T., & Primo-Martín, C. (2011). Interplay Between Product Characteristics, Oral Physiology And Texture Perception Of Cellular Brittle Foods. *Journal of Texture Studies*, *42*(2), 82–94. https://doi.org/10.1111/j.1745-4603.2010.00273.x

Wang, X., Wang, X., Upadhyay, R., & Chen, J. (2019). Topographic study of human tongue in relation to oral tribology. *Food Hydrocolloids*, *95*(April), 116–121. https://doi.org/10.1016/j.foodhyd.2019.04.022

Wilkinson, C., Dijksterhuis, G. B., & Minekus, M. (2000). From food structure to texture. *Trends in Food Science and Technology*, *11*(12), 442–450. https://doi.org/10.1016/S0924-2244(01)00033-4

Figure Captions

Figure 1: (a) Schematic representation of the experimental set-up; Pictures of (b) the polyvinyl alcohol artificial tongue model (ATM) and (c) the ATM topped with a food gel.

Figure 2: (a) A typical *rf* signal, composed of two main echoes: E_0 for the tongue-food interface, E_1 for the food-palate interface; (b) Ultrasound M-mode imaging of the entire set of signals obtained during an experiment and (c) Variation of ToF and R* (calculated on the basis of E_0) during a compression.

Figure 3: Estimation of the tongue deformation (without food) by ultrasound time of flight and texture analyzer.

Figure 4: (a) Force and (b) estimated ATM deformation over time as food gels were compressed on the soft ATM (C_2R_2); (c) Force and (d) estimated ATM deformation over time as food gels were compressed on the hard ATM (C_6R_2). The cloud around each line represents the standard deviation; at least six replicates were performed for each experimental test. The markers of different shapes were used to enhance the readability of the graphs. The dotted line on ATM deformation plot represents the maximum deformation imposed by the texture analyzer.

Figure 5: Force and estimated ATM deformation following compression (time t_1) for the experimental tests conducted with all the food gel types on ATMs differing in rigidity (C_2R_2 = soft and C_6R_2 = hard). Each color corresponds to a certain food gel type, whereas the two symbols distinguish between the ATM types.

Figure 6: Effect of surface roughness on estimated ATM deformation during the compression of the food gels (a) $Ge_{3.5}$ and (b) Ge_7. The cloud around each line represents the standard deviation.

Figure 7: (a) R* values during the compression of the food gels on the soft ATM (C_2R_2); the cloud around each line represents the standard deviation; the markers of different shapes were used to enhance the readability of the graphs. (b) R* values before compression began (t_0), and after compression ended (t_1), and the difference between the two (t_0-t_1). The error bars represent the standard deviations.

Figure 8: Effect of ATM rigidity on R* during the compression of the food gels on (a) the soft ATM (C_2R_2) and (b) the hard ATM (C_6R_2). The error bars represent the standard deviations.

Figure 9: Effect of surface roughness on R* during the compression of the food gels (a) $Ge_{3.5}$, (b) Ge_7, and (c) Ge_{7T}. The cloud around each line represents the standard deviation.

Tables

Table 1: Description of the food gels (Diameter: 30 mm; Height: 10 mm): composition (they all contained 15% wt of sucrose), Young's modulus values, and water-release capacity. Standard deviations are provided when applicable.

Table 2: Description of the ATMs (Diameter: 50 mm; Height: 20 mm): Young's modulus values, surface roughness profiles, and water-release capacity. Standard deviations are provided when applicable.

Figure 1

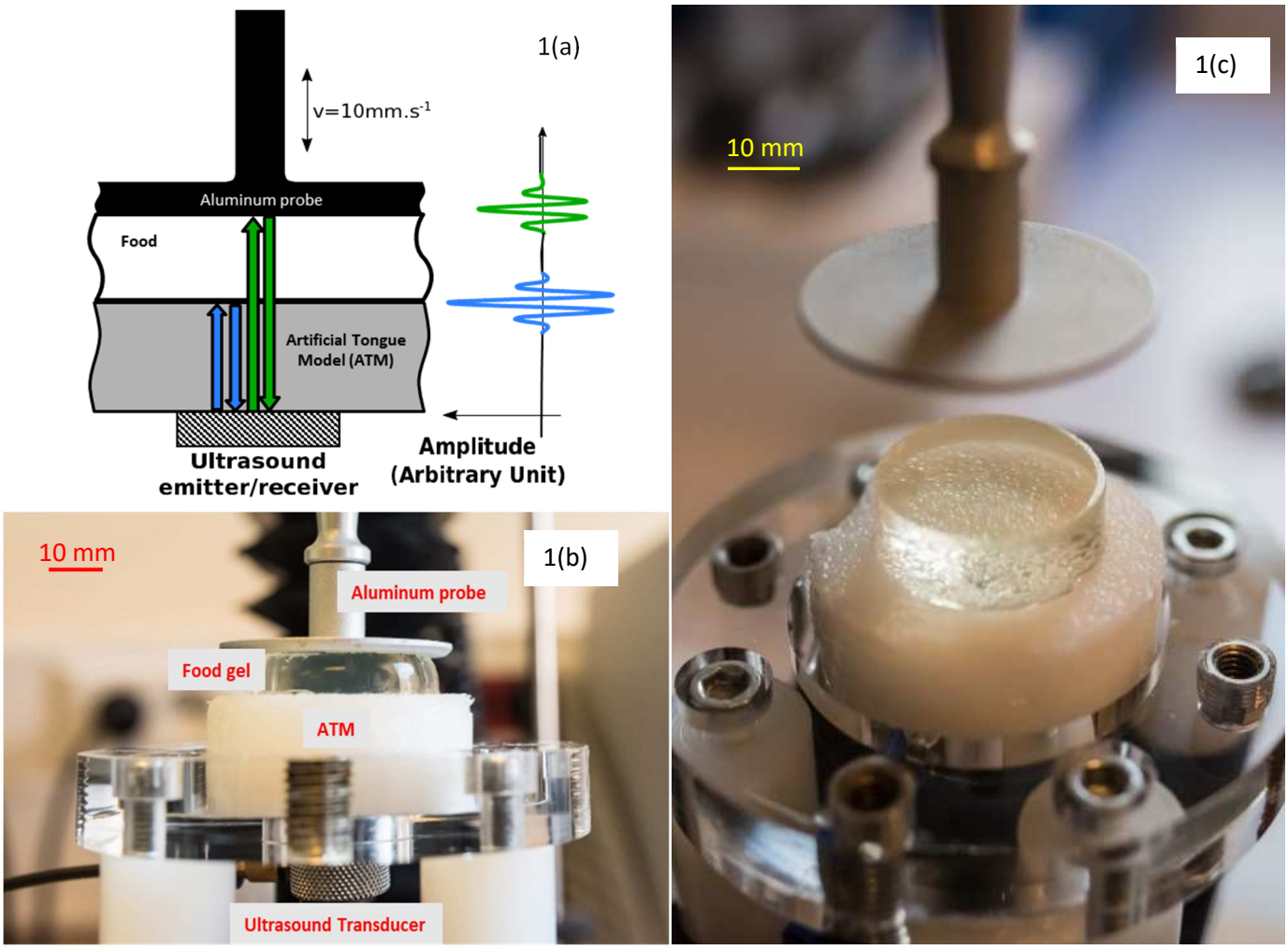
1(a)
v=10mm.s-1
Aluminum probe
Food
Artificial Tongue Model (ATM)
Ultrasound emitter/receiver
Amplitude (Arbitrary Unit)
1(b)
10 mm
Aluminum probe
Food gel
ATM
Ultrasound Transducer
1(c)
10 mm

Figure 2

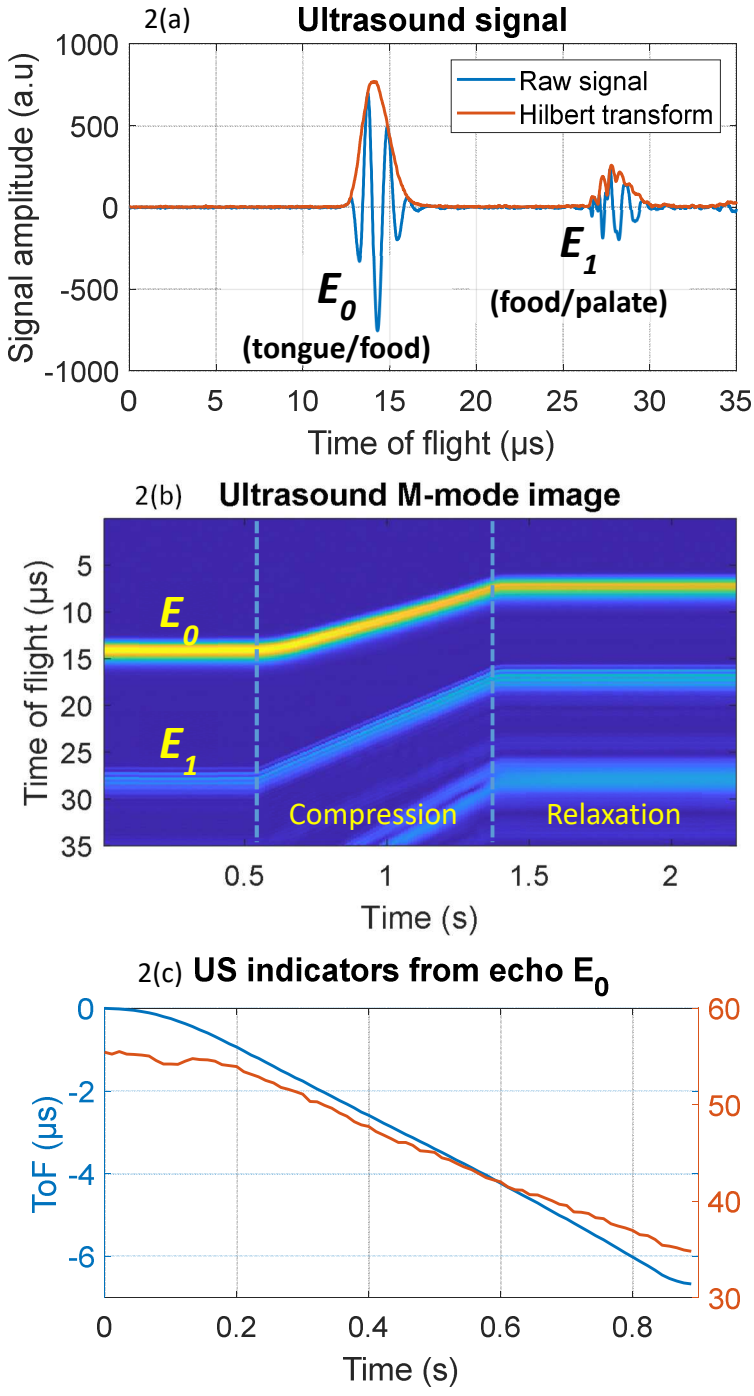
2(a)
Ultrasound signal
Raw signal
Hilbert transform
Signal amplitude (a.u)
Time of flight (µs)
E0
(tongue/food)
E1
(food/palate)
2(b)
Ultrasound M-mode image
Time of flight (µs)
Time (s)
Compression
Relaxation
2(c) US indicators from echo E0
ToF (µs)
R* (%)
Time (s)

Figure 3

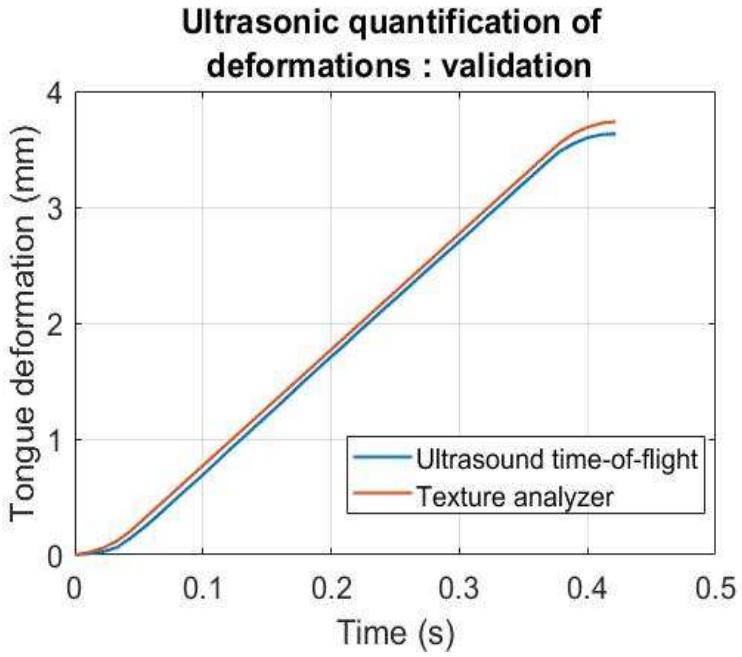
Ultrasonic quantification of deformations : validation
Tongue deformation (mm)
Time (s)
Ultrasound time-of-flight
Texture analyzer
0
1
2
3
4
0
0.1
0.2
0.3
0.4
0.5

Figure 4

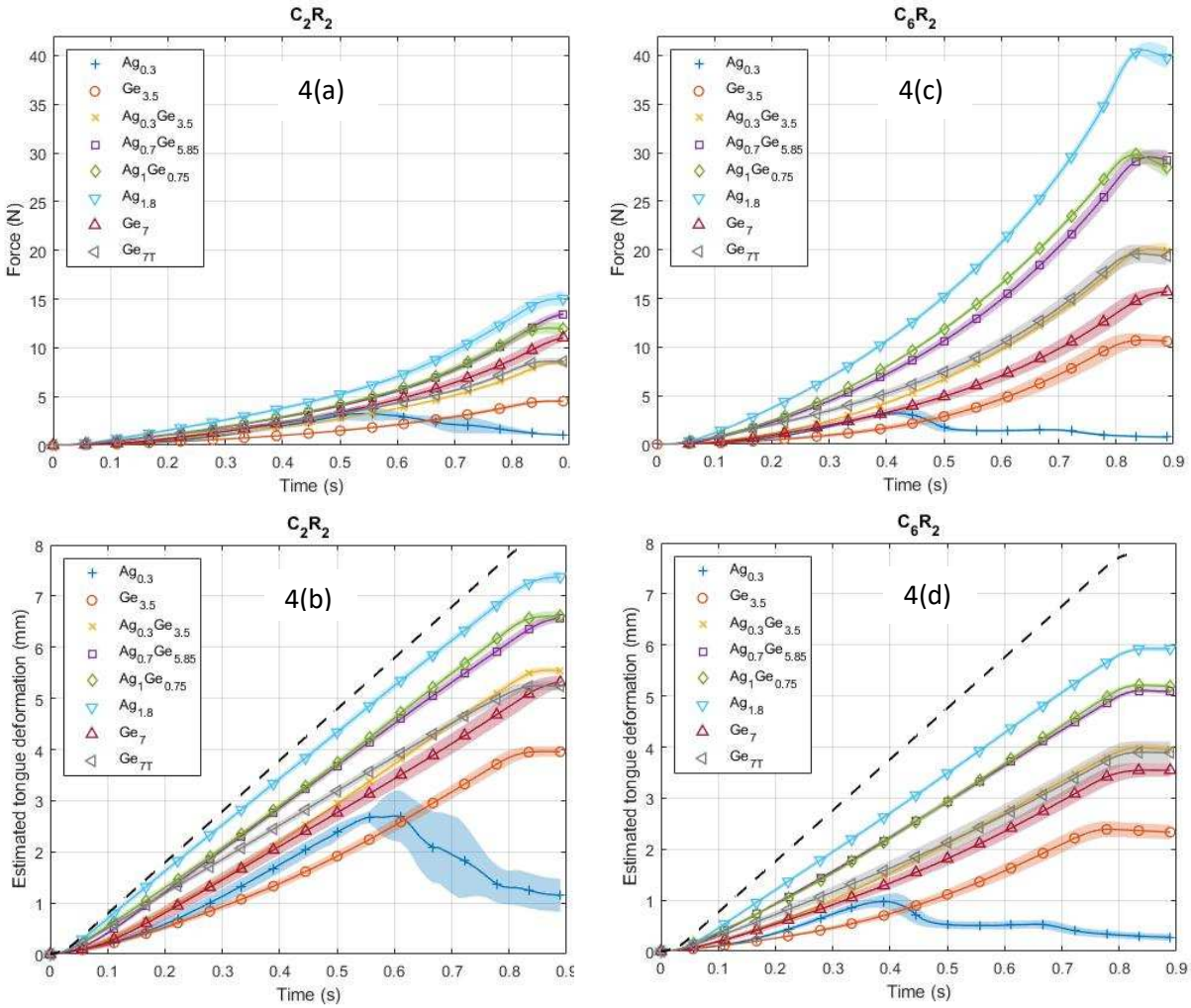
C2R2
4(a)
Force (N)
Time (s)
C6R2
4(c)
Force (N)
Time (s)
C2R2
4(b)
Estimated tongue deformation (mm)
Time (s)
C6R2
4(d)
Estimated tongue deformation (mm)
Time (s)
Ag0.3
Ge3.5
Ag0.3Ge3.5
Ag0.7Ge5.85
Ag1Ge0.75
Ag1.8
Ge7
Ge7T

Figure 5

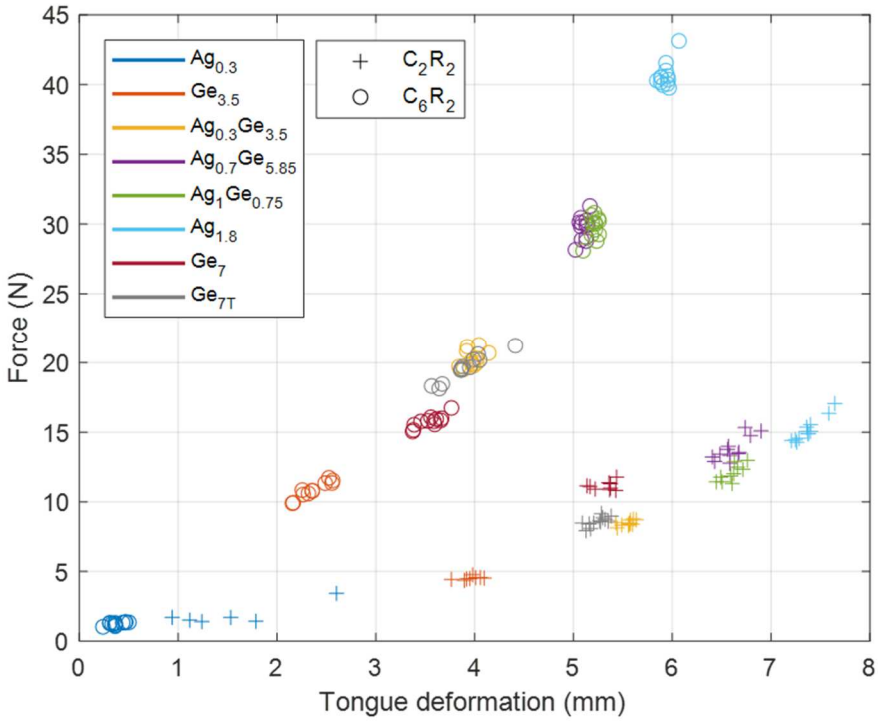
Ag0.3
Ge3.5
Ag0.3Ge3.5
Ag0.7Ge5.85
Ag1Ge0.75
Ag1.8
Ge7
Ge7T
C2R2
C6R2
Force (N)
Tongue deformation (mm)
0
5
10
15
20
25
30
35
40
45
0
1
2
3
4
5
6
7
8

Figure 6

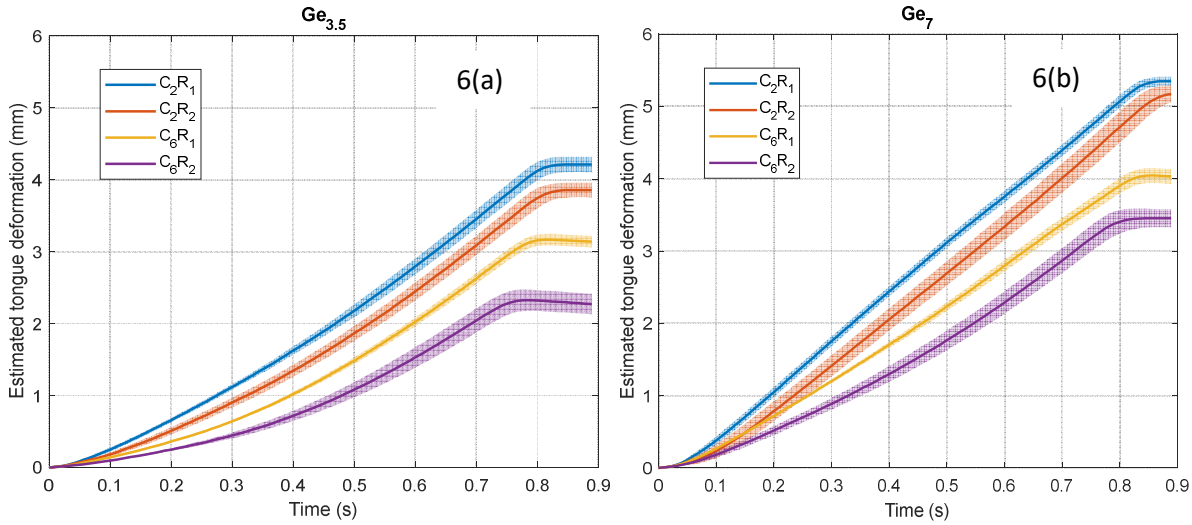
Ge3.5
6(a)
C2R1
C2R2
C6R1
C6R2
Estimated tongue deformation (mm)
Time (s)
Ge7
6(b)
C2R1
C2R2
C6R1
C6R2
Estimated tongue deformation (mm)
Time (s)

Figure 7

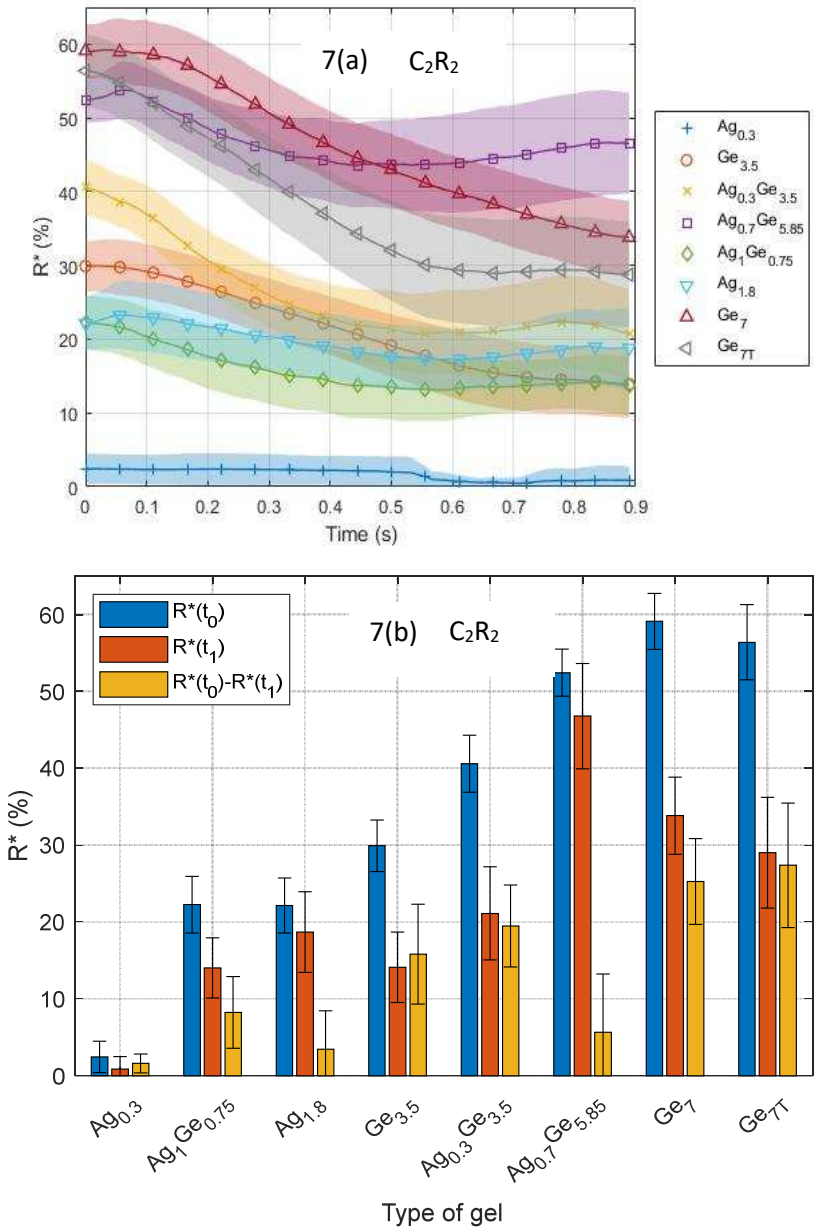
7(a) C2R2
R* (%)
Time (s)
Ag0.3
Ge3.5
Ag0.3Ge3.5
Ag0.7Ge5.85
Ag1Ge0.75
Ag1.8
Ge7
Ge7T
7(b) C2R2
R*(t0)
R*(t1)
R*(t0)-R*(t1)
R* (%)
Ag0.3
Ag1Ge0.75
Ag1.8
Ge3.5
Ag0.3Ge3.5
Ag0.7Ge5.85
Ge7
Ge7T
Type of gel

Figure 8

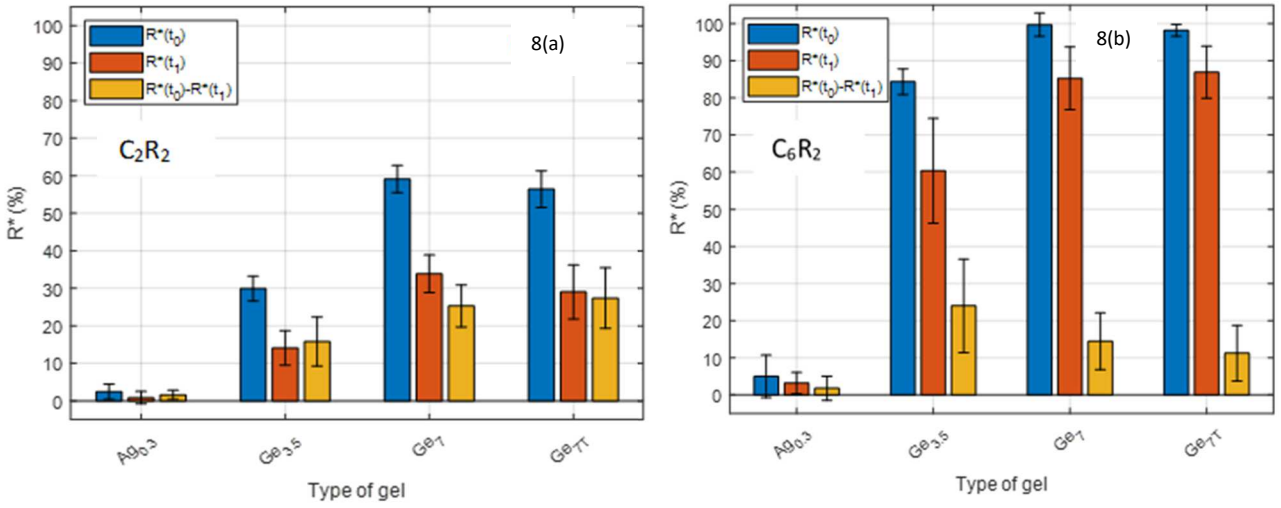
8(a)
C_2R_2
R*(t0)
R*(t1)
R*(t0)-R*(t1)
R* (%)
Type of gel
$Ag_{0.3}$
$Ge_{3.5}$
Ge_7
Ge_{7T}
8(b)
C_6R_2
R*(t0)
R*(t1)
R*(t0)-R*(t1)
R* (%)
Type of gel
$Ag_{0.3}$
$Ge_{3.5}$
Ge_7
Ge_{7T}

Figure 9

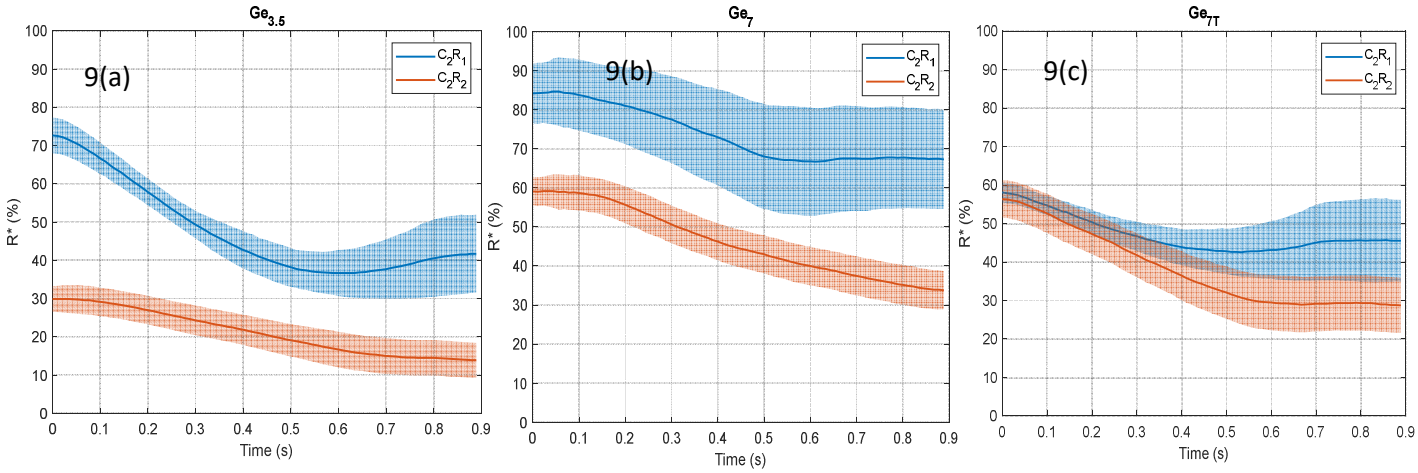
Ge3.5
9(a)
C2R1
C2R2
R* (%)
Time (s)
Ge7
9(b)
C2R1
C2R2
R* (%)
Time (s)
Ge7T
9(c)
C2R1
C2R2
R* (%)
Time (s)

Table 1

Gel type	Composition (% wt)				Young's modulus (kPa)	Water released (g)
	Water	Agar	Gelatin	TWEEN 20		
$Ag_{0.3}$	84.7	0.3	-	-	4 ± 3	0.150 ± 0.020* (without compression)
$Ag_1Ge_{0.75}$	83.25	1	0.75	-	58 ± 15	0.257 ± 0.020
$Ag_{1.8}$	83.2	1.8	-	-	132 ± 10	0.151 ± 0.012
$Ge_{3.5}$	81.5	-	3.5	-	2 ± 0.1	0.028 ± 0.002
$Ag_{0.3}Ge_{3.5}$	81.2	0.3	3.5	-	13 ± 3	0.029 ± 0.004
$Ag_{0.7}Ge_{5.85}$	78.45	0.7	5.85	-	32 ± 7	0.015 ± 0.003
Ge_7	78	-	7	-	24 ± 2	0.015 ± 0.002
Ge_7T	76.5	-	7	1.5	17 ± 2	0.012 ± 0.001

Table 2

ATM type	No. of freezing/ thawing cycles	Young's modulus (kPa)	Surface profile (µm)		Water released (g)
			Peak height (R_a)	Correlation length (β)	
C_2R_1	2	23 ± 1	42 ± 1	289 ± 36	0.022 ± 0.002
C_2R_2	2	18 ± 1	72 ± 14	435 ± 62	0.031 ± 0.003
C_6R_1	6	71.2 ± 1	55 ± 3	341 ± 62	0.015 ± 0.002
C_6R_2	6	71 ± 2	103 ± 3	429 ± 63	0.018 ± 0.003